Journal of Photochemistry and Photobiology A: Chemistry 228 (2012) 1–7

Contents lists available at SciVerse ScienceDirect

Journal of Photochemistry and Photobiology A: Chemistry

journal homepage: www.elsevier.com/locate/jphotochem

Parameters controlling the photocatalytic performance of ZnO/Hombikat TiO_2 composites

Mohamed S. Hamdy[a,b], Patrick Nickels[a,b], Islam H. Abd-Elmaksood[c], Hang Zhou[a,b], E.H. El-Mossalamy[c], Abdulrahaman O. Alyoubi[c], Stephen Lynch[b], Arokia Nathan[b], Geoff Thornton[b,*]

[a] Bio Nano Consulting Ltd., 338 Euston Road, London NW1 3BT, UK
[b] London Centre of Nanotechnology, 17-19 Gordon Street, London WC1H 0AH, UK
[c] Chemistry Department, Faculty of Science, King Abdulaziz University, Jeddah 21589, Saudi Arabia

ARTICLE INFO

Article history:
Received 28 July 2011
Received in revised form 7 November 2011
Accepted 10 November 2011
Available online 20 November 2011

Keywords:
TiO_2
ZnO
Hombikat
Photodegradation
Photocatalyst

ABSTRACT

Commercial TiO_2 (Hombikat, UV-100) was impregnated with different loadings of zinc nitrate solution and subsequently calcined at different temperatures in order to obtain a stable homogeneous solid composite of ZnO/TiO_2. The prepared samples were characterized by X-ray powder diffraction (XRD), scanning electron microscopy (SEM), high resolution transmission electron microscopy (HR-TEM), UV–vis and Raman spectroscopy, inductively coupled plasma mass spectroscopy (ICP), X-ray photoelectron spectroscopy (XPS) as well as N_2 adsorption and desorption measurements. Results show that ZnO was incorporated within the TiO_2 crystals and did not form a separate bulky phase or metallic zinc. Moreover, the calcination temperature dramatically modifies the texture properties of the prepared samples compared with original Hombikat TiO_2. The photocatalytic performance of the prepared samples was evaluated by monitoring the degradation of methyl orange dye under black light illumination. Three main parameters were studied; ZnO loading, surface area and initial pH of the methyl orange solution. The variation in ZnO loading appears to have less influence on the catalytic activity than either the surface area or the pH.

1. Introduction

TiO_2 is one of the most highly performing and extensively investigated photocatalysts, utilised for the degradation of environmental contaminants [1–3]. It is reported that the photocatalytic activity of titania is highly influenced by factors including its phase structure, surface area and doping elements in its lattice. The major disadvantage of TiO_2 is its large band gap (>3 eV), which limits its photo-response to the UV part of solar spectrum (<400 nm). After years of research, the challenge still remains to improve the photocatalytic activity and efficiency of TiO_2, and to extend its photocatalytic activity into the visible part of the solar spectrum.

TiO_2 exists in three distinct crystallographic forms: anatase, rutile and brookite. It is generally accepted that anatase is more photocatalytically active than rutile [4]. The well-known Degussa P25, which contains a mixture of both phases (~75% anatase and 25% rutile) [4,5], has been shown to have higher photocatalytic activity than pure anatase [6]. One proposed mechanism explaining this enhanced efficiency is that the photo-generated electron–hole pair has a longer lifetime in this mixed phase, due to interfacial charge transfer between the two phases [2].

Recent evidence from an electron spin resonance study suggests that the photo-generated electrons are trapped in the anatase particles, while the holes are transferred from anatase to rutile [7]. Thus, the carrier recombination rate is reduced and the overall photo-generated carriers' lifetime is increased. Based on a similar charge transfer principle, the coupling of two different semiconductor oxides is suggested as an alternative way to achieve high photocatalytic activity catalyst. Recent examples can be found in a range of TiO_2 composite nanoparticles, including WO_3 [8], SnO_2 [9], Fe_2O_3 [10] and ZnO [11–14]. Of these, ZnO has been the most extensively studied metal oxide in recent years due to its exceptional electrical and optical properties [15,16]. With a band gap of 3.2 eV, ZnO has been used as a photocatalyst for water treatment. Its low cost synthesis method and its varieties of different nanomorphologies with different properties [17] have motivated this present study of the TiO_2/ZnO composite catalysts.

Previous research on the TiO_2/ZnO photocatalyst has investigated the influence of the zinc salt used to deposit ZnO, the morphology, the crystal structure and the extent of ZnO loading

* Corresponding author. Tel.: +44 020 7679 7979; fax: +44 020 7679 7463.
E-mail address: g.thornton@ucl.ac.uk (G. Thornton).

1010-6030/$ – see front matter © 2011 Elsevier B.V. All rights reserved.
doi:10.1016/j.jphotochem.2011.11.001

[11–14,18,19]. Although earlier work discounted the enhancement in photocatalytic activities of TiO_2 by ZnO [18], more recent work has found an enhancement at certain ZnO/TiO_2 ratios [20,21]. It has been suggested that charge transfer (due to the difference in the Fermi level) at the TiO_2/ZnO interface is the principal cause of the enhancement [20–22]. However, quantitative studies of the different parameters that can affect the overall photocatalytic process are still limited.

The aim of this work was to investigate three parameters that could affect the photocatalysts activity: the ZnO loading, the surface area of the photocatalyst and the pH of the initial methyl orange (MO) solution. We report the modification and the characterization of the commercially available highly photocatalytic active Hombikat UV-100 TiO_2 catalyst with different ZnO loading and compare sets of samples that are calcined at different temperatures. The photocatalytic activity of these samples is evaluated by monitoring the photocatalytic decolourization of aqueous MO.

2. Experimental/materials and methods

2.1. Sample preparation

In a typical synthesis, a solution of the stoichiometric quantity of zinc nitrate hexahydrate (98% purity from Sigma–Aldrich) dissolved in 20 mL deionized water was prepared. The solution was added dropwise to 4 g of TiO_2 Hombikat UV-100 (provided by Sachtleben GmbH, Germany), and mixed to form a wet paste. The paste was dried at 100 °C for 24 h, divided into equal portions, and finally calcined at different temperatures (100, 200, 300, 400, and 550 °C) for 4 h. ZnO/TiO_2 composites were prepared with different ZnO loadings of 0.1 wt% (H-0.1-*x*), 0.5 wt% (H-0.5-*x*), 1 wt% (H-1-*x*), 2 wt% (H-2-*x*), and 5 wt% (H-5-*x*) – where *x* is the calcination temperature. Finally, samples were sieved to eliminate nanoparticle agglomerates larger than 100 μm. Pure TiO_2 Hombikat samples were also prepared and analysed. One was "as-received", labelled H.O., the remainder were prepared by mixing H.O. with 20 mL of deionized water, followed by drying, and calcination by the method described above (labelled as H-M-*x*) (Table 1).

2.2. Sample characterization

2.2.1. Powder X-ray diffraction (XRD)

X-ray powder diffraction analysis of all the samples was determined at room temperature using a Philips PW 3040 DY640 diffractometer equipped with a graphite monochromator using Cu Kα radiation (λ = 0.1541 nm). The samples were scanned over a 2θ range of 10–80° in steps of 0.02°.

2.2.2. Electron microscopy and energy dispersive X-ray spectroscopy (EDS)

For verification of the morphology of the TiO_2/ZnO particles, field-emission scanning electron microscopy (SEM, Carl Zeiss XB 1540) at 5 kV acceleration voltage was employed. For further microanalysis of the structure and material composition the samples were imaged in a Jeol JEM-2010 transmission electron microscope (TEM). Energy-dispersive X-ray spectroscopy (EDS) was performed with an attached Oxford Instruments ISIS EDS detector at an acceleration voltage of 200 kV. The samples for electron microscopy were prepared by suspending 10 mg of the mixed oxide in 5 mL ethanol followed by ultrasonication for 5 min. 0.5 mL of the suspension was dropped on top of either a silicon substrate for SEM, or a copper mesh for TEM imaging and dried in air.

Table 1
The quantities of zinc nitrate hexahydrate used in the preparation of each of the ZnO/TiO_2 composite samples synthesised.

Sample	Mass of $Zn(NO_3)_2{\cdot}6H_2O$ (mg)
H-0.1-*x*	14
H-0.5-*x*	73
H-1-*x*	146
H-2-*x*	292
H-5-*x*	730

2.2.3. UV–vis diffuse reflectance

UV–vis diffuse reflectance measurements were carried out at room temperature and performed on a PerkinElmer Lambda 950 spectrometer equipped with an integrating sphere to test absorption shifts in the wavelength range from 300 to 500 nm.

2.2.4. Raman spectroscopy

The laser Raman spectra were obtained by using a Renishaw Raman imaging microscope, system 2000. The green (λ = 514 nm) polarized radiation of an argon-ion laser beam of 20 mW was used for excitation. Spectra were collected in the range 100–1200 cm^{-1}.

2.2.5. Inductively coupled plasma mass spectroscopy (ICP)

The elemental analysis was carried out as follows: 0.4 g of each sample was dissolved in 16 mL H_2SO_4 and 6.4 g $(NH_4)_2SO_4$ by heating on a hot plate at 250 °C. Samples were cooled, diluted and analysed on Horiba Jolin Yvon Ultima-2 ICP using commercial standard solutions for calibration.

2.2.6. Specific surface areas (BET) and porosity measurements

The BET surface area analysis was made using a Tristar 3000 Micrometrics instrument, and the software used was the Tristar 3000 v6.04. The Micromeritics Tristar 3000 Analyser uses physical adsorption and capillary condensation principles to obtain information about the surface area and porosity of a solid material.

2.2.7. X-ray photoelectron spectroscopy (XPS)

The XPS spectra were recorded using a Kratos Axis Ultra spectrometer employing a monochromated Al Kα X-ray source and an analyser pass energy of 80 eV (wide scans) or 20 eV (narrow scans) resulting in a total energy resolution of ca. 1.2 and 0.6 eV, respectively. Uniform charge neutralisation of the photoemitting surface was achieved by exposing the surface to low energy electrons in a magnetic immersion lens system (Kratos Ltd.). The system base pressure was 5×10^{-1} mbar. Spectra were analysed by first subtracting a Shirley background and then obtaining accurate peak positions by fitting peaks using a mixed Gaussian/Lorenzian (30/70) line shape. During fitting, spin–orbit split components were constrained to have identical line width, elemental spin–orbit energy separations and theoretical branching ratios.

2.3. Photocatalysis study

Photocatalytic activity measurements were carried out in a home-built reactor. The reactor is a wooden box with dimensions of 100 cm height, 100 cm width, and 60 cm thickness, equipped with a 12 V transformer for an electric exhaust fan. Six 18 W black-light lamps (60 cm × 2.5 cm) of approximately 350–400 nm (F20 T8 BLB) were used; the total power of the UV light at the surface of the test suspension measured with a Newport 918D-UV-OD3 detector and power meter was 13 W/m^2. In a typical experiment, 100 mL of aqueous MO solution (10 mg/L) was stirred (300 rpm) with 100 mg of the different photocatalysts. Samples were withdrawn at 15 min intervals, filtered through a 0.2 mm PTFE Millipore membrane filter to remove suspended catalyst agglomerates, and finally analysed using the UV–vis spectrometer in the range between 250 and 600 nm.

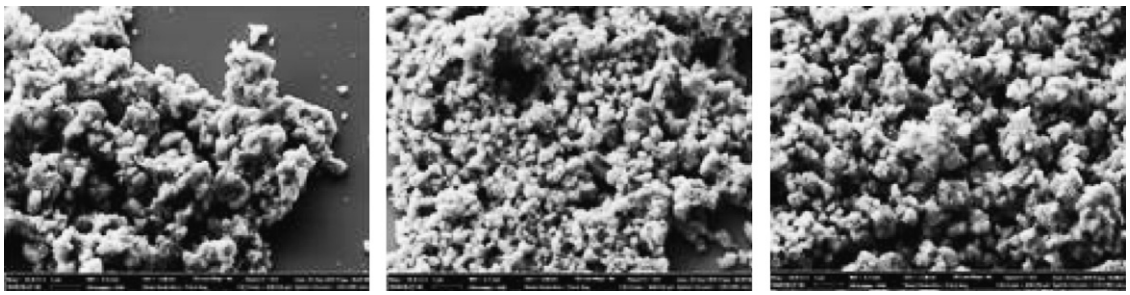

Fig. 1. SEM images of the (a) original Hombikat TiO_2; (b) calcined Hombikat TiO_2; (c) Hombikat TiO_2 with 5% ZnO loading.

3. Results

3.1. Structure and morphology

Optical inspection of the synthesised nanoparticles showed that they were still white in colour, with a significant reduction on the "light powder" texture characteristic of the Hombikat. SEM images of the H.O., H-M-550, and H-5-550 are shown in Fig. 1a–c, respectively. These images indicate that ZnO addition and heat treatment do not give rise to changes on the micrometer scale when compared with "as received" Hombikat powder.

The powder X-ray diffraction patterns of different TiO_2 photocatalysts (Fig. 2) showed that all samples are present in the anatase phase; peaks characteristic of anatase are located at 2θ values of 25°, 48°, 45° and 55° [23,24]. The characteristic peaks of rutile at 2θ values of 27° and 36° [23] are absent, which indicates that samples retained their original phase during calcination. Moreover, the crystallinity of the pure Hombikat sample (H.O.) was drastically improved by the effect of thermal treatment as evidenced by the sharper reflections. In addition, the XRD measurements did not exhibit any characteristic peaks of ZnO, indicating an absence of any bulky crystalline ZnO particles. The Raman data also show evidence of the anatase phase purity as well the improved crystallinity following calcinations (for details see the Supplementary Information).

To confirm the ZnO concentration in the synthesised materials, a full elemental analysis was carried out before and after the synthesis. Table 2 shows the theoretical amount of ZnO (wt%) added to TiO_2 samples during the synthesis compared with the actual amounts as obtained from ICP analysis in the final products. The difference between the theoretical and the actual ZnO weight percentage in each of the samples can be attributed to partial loss of sample during the sieving procedure. The results show that ZnO was incorporated in the final solid product with a ZnO/TiO_2 ratio comparable to the theoretical ratio determined at the outset. Different trace elements were also found at ppm levels, which most likely are contaminants from the original chemicals used for the synthesis.

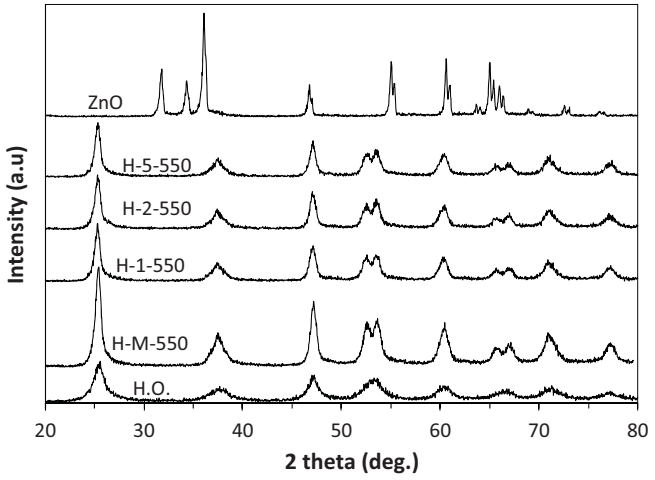

Fig. 2. XRD patterns of the prepared samples compared with ZnO.

Table 2
The elemental analysis as obtained by the ICP technique.

Sample	ZnO[a] (wt%)	ZnO[b] (wt%)	Trace elements (ppm)				
			Cd	Co	Cr	Fe	Pb
H.O.	0	<0.1	1.9	431	16	<1	215
H-M-550	0	<0.1	4.9	469	22	<1	218
H-0.1-550	0.1	0.19	3.3	414	18	<1	253
H-0.5-550	0.5	0.44	10	495	29	<1	240
H-1-550	1	0.70	5.8	517	8	3.5	155
H-2-550	2	1.40	14	400	<1	46	368
H-5-550	5	3.94	5.4	541	4.5	127	466

[a] Theoretical amount.
[b] Actual amount.

The surface morphology of the catalyst was examined by N_2 adsorption–desorption measurements. Table 3 details the porosity measurements of the prepared samples calculated from the adsorption branch of the isotherms using the Barrett–Joyner–Halenda formula. The surface area of the original Hombikat sample was 317 $m^2\,g^{-1}$, which was the highest surface area of all the samples analysed. This feature of Hombikat is thought to arise from its mesoporous structure, and its low crystallinity phase as observed in the XRD analysis [25]. After thermal treatment (with and without ZnO additions) the surface area decreased by two thirds due to the collapse and reduction of the porous structure. This result is in good agreement with the results obtained from XRD patterns of the prepared samples. Moreover, the pore sizes of the thermally prepared samples were at least two times greater than the original Hombikat material.

Fig. 3 compares the effect of calcination temperature on the texture of the 0.5 wt% ZnO/TiO_2 series. The surface areas of the prepared samples decreased dramatically with increasing the calcination temperature (100–550 °C). Conversely, the pore sizes increased in size with increasing calcination temperature.

Table 3
The texture properties of the prepared samples as obtained by N_2 physisorption.

Sample	Surface area ($m^2\,g^{-1}$)	Pore volume (cm^3/g)	Pore size (nm)
H.O.	317.68	0.34	5.6
H-M-550	71.08	0.264	11.66
H-0.1-550	69.80	0.257	11.61
H-0.5-550	67.71	0.255	11.98
H-1-550	65.04	0.249	12.12
H-2-550	65.57	0.298	13.38
H-5-550	61.32	0.299	14.21

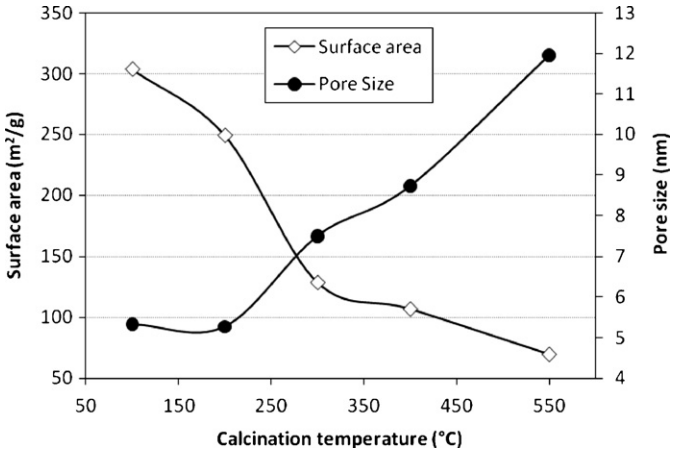

Fig. 3. The surface areas and the pore sizes of the 0.5 wt% ZnO/TiO_2 (H-0.5) series as a function of calcination temperature.

In an attempt to gain a deeper insight into the structural properties, TEM was performed and the micrographs are presented in Fig. 4. To see the changes in different steps of the modification, the original TiO_2 (H.O.) (Fig. 4a) has been compared with the TiO_2 calcined at 550 °C sample (H-M-550) (Fig. 4b) and the TiO_2 loaded with 5 wt% ZnO calcined at 550 °C (H-5-550) (Fig. 4c). Fig. 4a shows clearly the micro porous structure of H.O. indicated by the grainy appearance. Careful observations on the TEM screen reveal an agglomeration of crystallites with sizes of 30–50 nm. After calcination at 550 °C (Fig. 4b) the crystallites gain smooth surfaces and become more discernable, indicating the disappearance of micropores, which was also seen in the N_2 adsorption measurement results shown in Table 3. In addition, single lattice planes and fringe patterns of overlapping planes are visible in the TEM pictures for H-M-550 and H-5-550 (Fig. 4b and c), indicating an increase in crystallinity in these calcined samples. A comparison of the images in Fig. 4b and c, indicates that no significant changes seem to have been generated in the structural make up of the samples by the introduction of ZnO, consistent with the XRD results (Fig. 2).

In the electron microscope investigations, EDS spectroscopy was employed to confirm the material composition of the original and the modified materials. Scans of agglomerations in a range of 500 nm to 1 μm, consisting of about 50–400 crystallites, showed the existence of Zn in the loaded TiO_2. The exact location is difficult to identify due to a lack of crystalline ZnO present in these samples, indicated by the absence of typical ZnO peaks in XRD (Fig. 2) and in electron diffraction patterns. As a result, the modified TiO_2 in Fig. 4b and the ZnO loaded TiO_2 in Fig. 4c appear very similar, despite the presence of Zn.

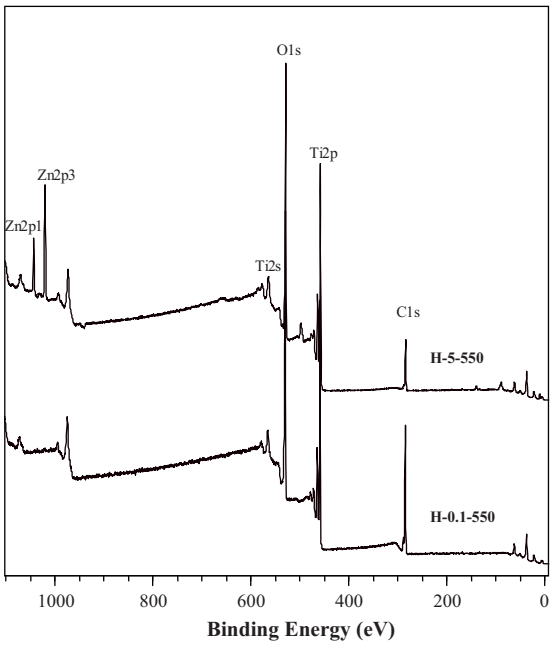

Fig. 5. XPS survey spectra of H-0.1-550 and H-5-550 samples.

XPS was used to explore the spatial relationship between ZnO and TiO_2. Fig. 5 shows the XPS spectra for only H-0.1-550 and H-5-550 for simplification (see Supplementary Information for the full data set). For all the samples, Ti_{2p} scans indicate the presence of TiO_2 in the near surface. The C_{1s} and O_{1s} scans are very similar for the majority of the samples. Whereas similar O_{1s} peaks appear due to similar energy of signals from Zn–O and Ti–O, it should be noted that the C peak arises mainly from contamination within the instrument.

The binding energy of $Zn_{2p3/2}$ was determined to be 1021.71 eV, which is consistent with ZnO or a mixed Zn oxide. Based on the peak area ratio; the Zn/Ti ratio was much higher than the designed doping concentration, and because of the small penetration depth in XPS measurements (about 10 nm) it can be concluded that the ZnO is mainly located on the surface of TiO_2 particles. Together with the EDS data, which indicate that ZnO is dispersed on the particles, this suggests that there is a thin layer of ZnO formed on the surfaces of the TiO_2 particles.

3.2. The photocatalytic performance

The photocatalytic activity of each of the samples was tested by monitoring the photo-degradation of methyl orange dye as a

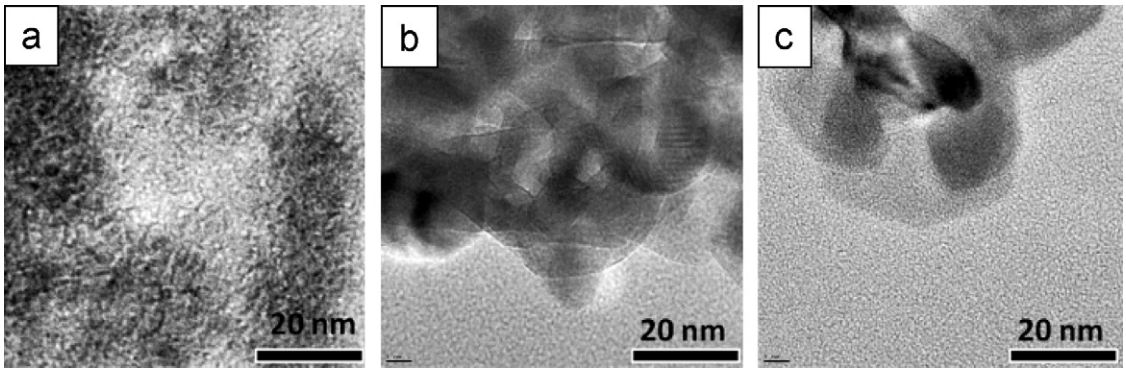

Fig. 4. TEM images of (a) H.O., (b) H-M-550 and (c) H-5-550. All three materials contain 30–50 nm large crystallites. After calcination the grainy micro porous structure of (a) disappears and lattice planes become visible in (b) and (c) due to increased crystallinity.

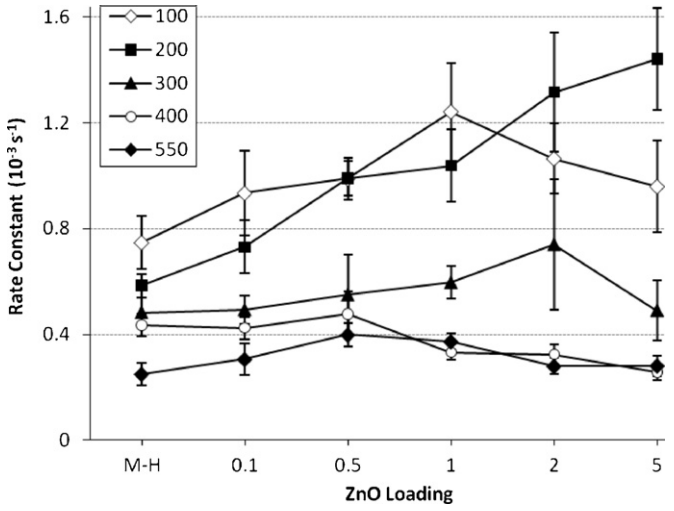

Fig. 6. Photocatalytic activity (rate constant) of samples calcined at different temperatures (100–550 °C) and against the loading of ZnO.

model compound. This was achieved by using the UV black-light box described in Section 2.3. The photoactivity profile of each TiO_2 sample was fitted assuming first order kinetics:

$$C_M = C_{Mo}e^{-kt} \quad (1)$$

where C_M is the concentration of methyl orange at time (t), C_{Mo} is the initial concentration, and k is the observed rate constant. Photocatalytic reactions are complex and the exact mechanisms are still a matter of debate [26], however using the first order model to follow the decay of the MO allows a fast and efficient comparison of the effect of the different ZnO loadings on TiO_2 on cleaning efficacy.

In order to understand the changes found in the observed rate constants, we have investigated the effects of the following three parameters: the calcination temperature and consequentially the surface area, the ZnO loading and the initial pH of the methyl orange solution.

Fig. 6 shows the observed rate constants from the decolourization experiments for the complete set of samples. All samples were tested three times to obtain mean error values, which are largest for the samples recorded to have higher rates of activity. The trend observed here is that as the calcination temperature increases, the photo-activity of the sample decreases. By recalling the XRD and BET results (see Figs. 2 and 3) this reduction in activity can be linked to an increase in crystallinity and a loss in surface area as the calcination temperature is increased. The data in Fig. 6 also indicate that the samples calcined at lower temperatures show an increase in observed rate constant as the amount of ZnO is increased. Higher photocatalytic activities were obtained for the samples containing high ZnO loading and calcined at 200 °C (H-2-200, and H-5-200).

A slight orange colour change was observed when the samples displaying high activity (H-2-200 and H-5-200) were added to the prepared MO solution, indicating a decrease of its pH. These solutions had a pH between 4.0 and 4.8, while the pH of the MO solution containing the original Hombikat (H.O.) was approximately 5.4 ± 0.2. An XPS analysis was used to determine if this reduced pH was the result of residual nitrate after calcination, i.e. that not decomposed according to the thermal transformation reaction of the zinc nitrate hexahydrate described by Kozak et al. [27]. Fig. 7 shows the XPS results for high %ZnO samples calcined at lower temperatures. A weak broad peak at 400.2 eV typical of N in an organic matrix is seen and a sharper peak at 407 eV corresponds to nitrate [28]. The XPS data for samples calcined at higher temperatures (not shown) do not exhibit a N 1s feature at 407 eV. Presumably the organic N resulted from the reaction of the nitrate

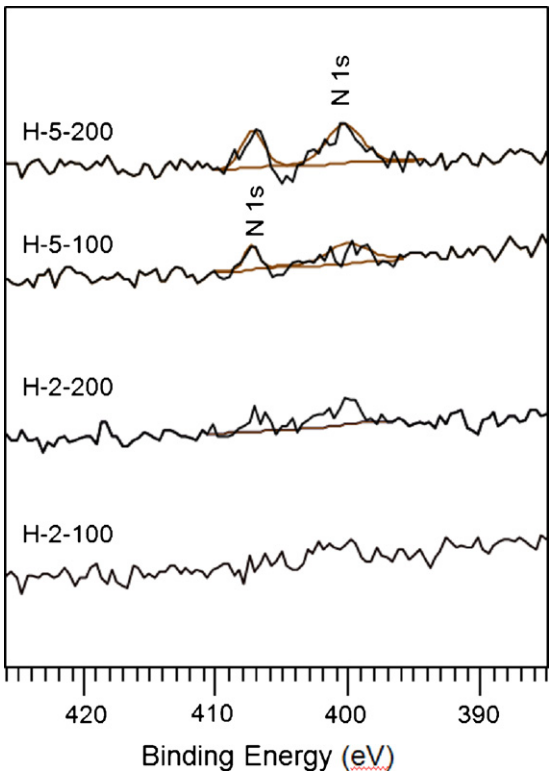

Fig. 7. XPS survey spectra of H-5-100/200 and H-2-100/200 samples. Spectra were recorded under the same conditions, including electron energy analyser pass energy and accumulation time.

with atmospheric organics. It is clear that some nitrate ions are still present due the partial transformation to ZnO. In aqueous solution this will lower the pH due to the formation of nitric acid.

An additional measurement of MO decolourisation was used to confirm the effect of pH on the photocatalytic performance. This employed an original Hombikat sample for which the pH was adjusted to 4.2 by addition of nitric acid.

Fig. 8 shows the comparison between the degradation of methyl orange when catalyzed by the original Hombikat at pH 4.2 (H.O. 4.2), the original Hombikat at pH 5.4 (H.O. 5.4), and the 5 wt% ZnO loaded Hombikat that has been calcined at 200 °C (H-5-200).

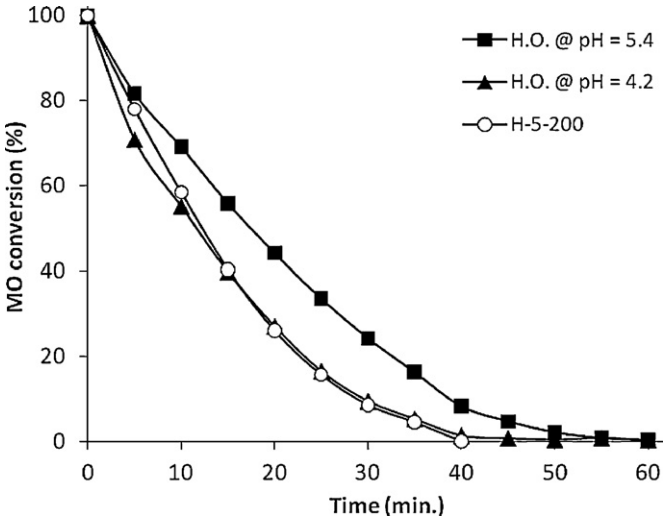

Fig. 8. A comparison between the MO degradation catalyzed by Hombikat at pH 4.2, Hombikat at pH 5.4, and with H-5-200.

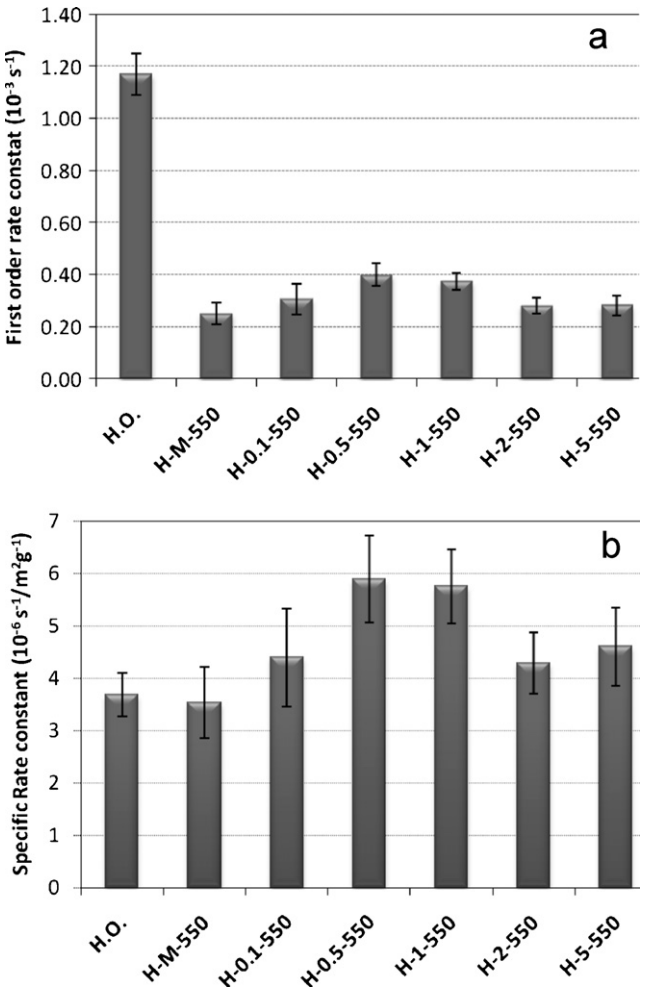

Fig. 9. (a) The observed first order rate constant of the original Hombikat and the samples calcined at 550 °C. (b) The specific photo-activity (first order rate constant from (a) per surface area) shows the effect of ZnO loading. The lack of a visible change in the methyl orange colour and the absence of a nitrate peak in XPS lead us to exclude the influence of pH on these results.

The photocatalytic activity for the H.O. 4.2 seems to be very similar to the H-5-200 and both are more active than the H.O. sample tested at a pH of 5.4, providing evidence that nitric acid formed in the solution by the nitrates present at the ZnO/TiO_2 nanocomposite surface does indeed enhance the rate of photocatalysis. This is consistent with trends observed for sulfate-modified titania nanoparticles in MO when the pH was lowered by additions of H_2O_2 [29]. This effect has been attributed to the enhancement of the adsorption of the anionic species present in the MO solution by the increase of positive charging of the nanoparticle surface [29,30].

Finally, we consider the effect of ZnO loading on the first order rate constants of samples with different ZnO loadings calcined at 550 °C. As previously mentioned, no residual nitrates were present on these samples, and consequently no significant effects of pH were observed on the MO solution. The results are shown in Fig. 9a, which indicate a maximum photoactivity at 0.5 wt% ZnO loading. However, the largest variation was found in the photocatalyst activities between the original (H.O.) and modified samples. The original Hombikat sample showed a much higher activity, which can be attributed to the dramatic decrease in surface area after calcination. To differentiate between the effect of ZnO loading and the effect of surface area, the data were normalised to surface area to give their specific photo-activity (see Fig. 9b).

The data in Fig. 9b indicates that the specific photo-activity of the original and the modified Hombikat samples are almost the same (in fact statistically the same when compared with H-M-550, H-0.1-550, H-2-550 and H-5-550). The only measurable differences with respect to the Hombikat powder (H.O.) is for samples H-0.5-550 and H-1-550. Hence, these data suggest that loadings of ZnO in the range of 0.5–1 wt% have a positive effect on the photocatalytic activity. Similar trends of maximum activity at low (0.5–1%) loading ratios have been reported [19]. We found that the effect of optimum ZnO loading (~0.5%) resulted in a rate increase of 20–30% over the Hombikat sample (H.O.).

The photo-catalytic activity of TiO_2 doped with ZnO has been reported several times [11–14]. The underlying mechanism of activity enhancement involves an increased charge carrier lifetime created by charge separation. ZnO has a similar band gap to anatase TiO_2 (3.2 eV) but a higher lying valence and conduction band [31], leading to charge transfer at the interface. Electrons and holes are generated upon irradiation of ZnO and TiO_2 with band gap light, with hole transfer from anatase to ZnO and electron transfer from ZnO to TiO_2 forming $^{\bullet}OH$ radicals in the surrounding water. Thus, the photocatalytic activity of TiO_2 is improved by loading it with ZnO. In our experiments, we found a maximum photo-activity when TiO_2 was loaded with ~0.5 wt% ZnO. It is thought that not enough interfaces are produced at lower loadings to significantly enhance charge separation. ZnO particles on the TiO_2 surface could behave as new centres of recombination at high loadings of ZnO. An alternative explanation for the decreased activity at higher loadings is that a thicker ZnO coating suppresses a balance of simultaneous oxidation and reduction [31]. In the present work, the ZnO loading is found to produce a significant modification of the photocatalytic behaviour, although the surface area and pH produce a much larger effect.

4. Conclusions

TiO_2 was impregnated with different loadings (from 0.1 up to 5 wt%) of ZnO using a wet chemical technique. Characterization by XRD, SEM, HR-TEM, UV–vis and Raman spectroscopy, ICP, XPS and N_2 adsorption and desorption measurements indicate that ZnO does not incorporate as separate bulky crystals. Moreover, the measurements are not consistent with the presence of a substantial ZnO film. The calcination temperature changes the surface area, with a lower surface area at higher calcination temperature leading to a lower photocatalytic activity. A lower calcination temperature results in incomplete nitrate removal during calcination and a consequent decrease in pH of the photocatalysis test solution. After excluding the effects produced by surface area, pH and changes of zinc salts, a maximum in activity was obtained at ~0.5 wt% ZnO/TiO_2 for samples calcined at 550 °C. Although the influence of ZnO is observed, the effect is much smaller than that claimed in recent work [11,16].

Acknowledgements

The authors thank Tony Osborne, UCL for ICP analysis, Zlatko Saracevic, Department of Chemical Engineering and Biotechnology, University of Cambridge for BET measurements, Dr. Paul Wincott, School of Earth, Atmospheric and Environmental Sciences, University of Manchester for XPS analysis, Dr. Felicity Sartain for valuable discussions and the Deanship of Scientific Research at King Abdulaziz University for the support of this project (T/80/429).

Appendix A. Supplementary data

Supplementary data associated with this article can be found, in the online version, at doi:10.1016/j.jphotochem.2011.11.001.

References

[1] D. Bahnemann, Solar Energy 77 (2004) 445–459.
[2] L. Kavan, M. Grätzel, S.E. Gilbert, C. Klemenz, H.J. Scheel, Journal of the American Chemical Society 118 (1996) 6716–6723.
[3] B. Sun, P.G. Smirniotis, Catalysis Today 88 (2003) 49–59.
[4] R.I. Bickley, T. Gonzalez-Carreno, J.S. Lee, L. Palmisano, R.J.D. Tilley, Journal of Solid State Chemistry 92 (1991) 178–190.
[5] T. Ohno, K. Sarukawa, K. Tokieda, M. Matsumura, Journal of Catalysis 203 (2001) 82–86.
[6] S. Bakardjieva, J. Subrt, V. Stengl, M. Dianez, M. Sayagues, Applied Catalysis B: Environmental 58 (2005) 193–202.
[7] D.C. Hurum, A.G. Agrios, K.a. Gray, T. Rajh, M.C. Thurnauer, The Journal of Physical Chemistry B 107 (2003) 4545–4549.
[8] T. Ohno, F. Tanigawa, K.A. Fujihara, S. Izumi, M. Matsumura, Journal of Photochemistry and Photobiology A: Chemistry 118 (1998) 41–44.
[9] L. Shi, C.Z. Li, H.C. Gu, D.Y. Fang, Materials Chemistry and Physics 62 (2000) 62–67.
[10] B. Pal, M. Sharon, G. Nogami, Materials Chemistry and Physics 59 (1999) 254–261.
[11] D. Liao, C. Badour, B. Liao, Journal of Photochemistry and Photobiology A: Chemistry 194 (2008) 11–19.
[12] M. Vaezi, Journal of Materials Processing Technology 205 (2008) 332–337.
[13] Z. Zhang, Y. Yuan, Y. Fang, L. Liang, H. Ding, L. Jin, Talanta 73 (2007) 523–528.
[14] N. Daneshvar, D. Salari, A.R. Khataee, Journal of Photochemistry and Photobiology A: Chemistry 162 (2004) 317–322.
[15] U. Ozgur, Y.I. Alivov, C. Liu, A. Teke, M.A. Reshchikov, S. Dogan, V. Avrutin, S. Cho, H. Morkoc, Journal of Applied Physics 98 (2005) 041301.
[16] V. Kandavelu, H. Kastien, K. Ravindranathan Thampi, Applied Catalysis B: Environmental 48 (2004) 101–111.
[17] Z.L. Wang, Journal of Physics: Condensed Matter 16 (2004) R829–R858.
[18] G. Marcì, V. Augugliaro, M.J. López-Muñoz, C. Martín, L. Palmisano, V. Rives, M. Schiavello, R.J.D. Tilley, A.M. Venezia, The Journal of Physical Chemistry B 105 (2001) 1033–1040.
[19] H. Wang, Z. Wu, Y. Liu, Z. Sheng, Journal of Molecular Catalysis A: Chemical 287 (2008) 176–181.
[20] S. Chen, W. Zhao, W. Liu, S. Zhang, Applied Surface Science 255 (2008) 2478–2484.
[21] J. Tian, J. Wang, J. Dai, X. Wang, Y. Yin, Surface & Coatings Technology 204 (2009) 723–730.
[22] Y. Ku, Y-H. Huang, Y.-C. Chou, Journal of Molecular Catalysis A 342–343 (2011) 18–22.
[23] B. Li, X.H. Wang, M. Yan, L. Li, Materials Chemistry and Physics 78 (2002) 184–188.
[24] K. Lee, S. Kim, J. Song, J. Lee, Y. Chung, S. Park, Journal of the American Ceramic Society 85 (2002) 341–345.
[25] G. Colon, M.C. Hidalgo, J.A. Navio, Journal of Photochemistry and Photobiology A: Chemistry 138 (2001) 79–85.
[26] D. Friedmann, C. Mendive, D. Bahnemann, Applied Catalysis B: Environmental 99 (2010) 398–406.
[27] A.J. Kozak, K. Wieczorek-Ciurowa, A. Kozak, Journal of Thermal Analysis and Calorimetry 74 (2003) 497–502.
[28] A. Krepelová, J. Newberg, T. Huthwelker, H. Bluhm, M. Ammann, Physical Chemistry Chemical Physics 12 (2010) 8870–8880.
[29] K.M. Parida, N. Sahu, N.R. Biswal, B. Naik, a.C. Pradhan, Journal of Colloid and Interface Science 318 (2008) 231–237.
[30] S. Ahmed, M.G. Rasul, R. Brown, M.a. Hashib, Journal of Environment Management 92 (2011) 311–330.
[31] A. Fujishima, X. Zhang, D. Tryk, Surface Science Reports 63 (2008) 515–582.